



Human Connectome Mapping and Monitoring Using Neuronanorobots

Nuno R. B. Martins

Center for Mathematics
University of Minho

n-martins@n-martins.com

Wolfram Erlhagen

Center for Mathematics
University of Minho

wolfram.erlhagen@math.uminho.pt

Robert A. Freitas, Jr.

Institute for Molecular Manufacturing

rfreitas@rfreitas.com

Journal of Evolution and Technology - Vol. 26 Issue 1 – January 2016 - pgs 1-24

Abstract

Neuronanorobotics is the application of medical nanorobots to the human brain. This paper proposes three specific classes of neuronanorobots, named endoneurobots, gliabots and synaptobots, which together can non-destructively map and monitor the structural changes occurring on the 86×10^9 neurons and the 2.42×10^{14} synapses in the human brain, while also recording the synaptic-processed 4.31×10^{15} spikes/sec carrying electrical functional information processed in the neuronal and synaptic network.

1. Introduction

Preserving human brain information is essential for truly preserving human life. A crucial part of that precious information is structural in nature and is referred to as the *human connectome*, believed to be the processing framework for functional information. No currently available technological tool claims the capacity to preserve whole human brain structural and functional connectome information comprehensively with proper temporal and spatial resolution.

Any nonlethal kind of brain damage caused by neurological disorders can irreversibly damage the human brain, causing loss of precious information. Such loss may include loss of brain structural information, such as neural connectivity, or loss of brain functional information, such as neurotransmitter activity patterns. Loss of information might affect proper cellular and organ-level neurological functions, eventually altering higher mental states, personality, and ultimately individuality and self-awareness. The usual causes of information

loss are physical trauma and a variety of degenerative and viral disorders. Once destroyed and not previously preserved, such information cannot, even in principle, be recovered using current techniques, thus permanently diminishing patient health.

Medical technological tools and methods for monitoring, measuring, validating, and archiving comprehensive brain-related structural information are urgently necessary because current technologies do not provide the necessary temporal and spatial resolution requirements for preserving fundamental human brain information. For example, none of the current technologies, either destructive or non-destructive in nature, can monitor the whole human brain *in vivo*, in real-time, with adequate cellular and subcellular temporal and spatial resolution for mapping the brain structural and functional electrical connectome with appropriate detail.

Medical nanorobotics technology, a medical technology first examined technically in the *Nanomedicine* book series (Freitas 1999, 2003), is expected to permit measuring, mapping, and monitoring structural and functional human brain information along with many other medical applications (Freitas 1998, 2000, 2003, 2005a, 2005b, 2005c, 2006a, 2006b, 2007, 2010; Morris 2001; Astier et al. 2005; Patel et al. 2006; Park et al. 2007; Popov et al. 2007; Martel et al. 2009; Mallouk and Sen 2009; Kostarelos 2010; Mavroides and Ferreira 2011). Neuronanorobotics, involving a specific class of medical nanorobots, is expected to permit *in vivo*, whole-brain, real-time mapping and monitoring of the relevant structural and functional cellular and sub-cellular brain information. Such nanorobots should, for example, permit mapping the whole human brain connectome (Sporns et al. 2005; Lu et al. 2009; Anderson et al. 2011; Kleinfeld et al. 2011; Seung 2011) by the coordinated activities of three primary types of cooperating neuronanorobots proposed here, to be called endoneurobots, gliabots, and synaptobots, as described below.

2. Structural and functional connectome-associated information

To comprehensively restore a brain to a proper healthy structural and functional state will likely require more than a simple connectomics neuro-synaptic diagram, as current neuroscience literature points to several other relevant forms of structural brain information. Consequently, medical technology might have to be capable of preserving information at the cellular and subcellular level, performing the following tasks:

- detecting and characterizing each of the individual 86.06 ± 8.12 billion neurons (Azevedo et al. 2009; Herculano-Houzel 2009) with volumes from ~ 33.5 micron³ (for granule cell) up to $\sim 4.18 \times 10^6$ micron³ (for motor neurons);
- monitoring the loss of $\sim 100,000$ neurons a day (~ 1 per second) (Pakkenberg and Gundersen 1997; Arking 2006);
- monitoring five phases of neuron genesis and elimination processes, occurring on time scales between 1-10 days (Gross 2000);
- monitoring the activity of the $84.61 \pm 9.83 \times 10^9$ glial cells (Azevedo et al. 2009);
- monitoring axon initial segment (typically the first 50 μm of axon) and axon hillock molecular characterization, particularly the quantification of Kv1 family potassium channel types responsible for shaping action potential waveforms, with turnover of ~ 3 hours (Lu et al. 2004; Palmer and Stuart 2006; Kole et al. 2007);
- monitoring the 10,000-52,000 micron long dendritic trees each having surface areas of 700-54,000 μm^2 (Donohue and Ascoli 2008);
- monitoring of dendritic development, establishment, and remodeling, and monitoring important neuron organelles, especially the neuron nucleus (diameter 4-100 μm); and
- monitoring intracellular compartments.

Comprehensive structural connectome monitoring might also require technology capable of detecting synaptic plasticity structural changes induced by synaptic cross-talk, such as synaptic based long-term potentiation, long-term depression, short-term plasticity, metaplasticity and homeostatic plasticity, as well as measuring the dynamic composition of the post-synaptic density, each having $\sim 10,000$ proteins comprising ~ 100 different types (Sheng and Hoogenraad 2007).

It is not clear if human brain functional information can be deduced solely from the underlying structural information, so functional information remains either essential or important in providing redundant measurement and inference for brain information preservation. Such functional information may include *in vivo* measurement of action potential associated electrical information; neurotransmitters, hormones, and neurotrophic-based extracellular communication (e.g., synaptic, paracrine, or endocrine signaling);

intracellular chemical communication (e.g., via GTP-binding proteins, second messenger molecules, protein kinases, ion channels, and other effector proteins); and molecular diffusion occurring in the 20 per cent of brain volume comprising the extracellular spaces (Thorne and Nicholson 2006; Sandberg and Bostrom 2008).

Intracellularly, it might be relevant to identify and quantitatively measure:

- neuron gene expression and transcription factors by monitoring the 20,000-25,000 protein-coding genes and 2.85 billion nucleotides (IHGSC 2004), with total information size of ~3.08 gigabytes (IHGSC 2004);
- neuron nucleus traffic of the 22,000-505,000 molecules of mRNA per neuron cell (Islam 2011);
- local protein synthesis and degradation in dendrites, axons and synapses;
- action-potential-induced openings of the ~20 Ca^{2+} channels present, on average, per each active zone, measuring consequent fast release with a delay 50-500 μsec (Sabatini and Regehr 1996; Südhof 2004);
- mechanisms of calcium wave propagation at velocity ~28 $\mu\text{m}/\text{sec}$ including diffusion of IP3 and extracellular ATP (velocity of ~41 $\mu\text{m}/\text{sec}$) (Newman 2001), among other functional and structural information, along with the resultant Ca^{2+} transient (lasting 400-500 μsec , with $a > 5 \mu\text{M Ca}^{2+}$) (Südhof 2004);
- the 17-500 nm diameter synaptic vesicles (average ~40 nm) (Qu et al. 2009; Südhof 2004), with the average lumen volume of 11,500 nm^3 in CNS (“typical” synaptic terminals have in the order of ~100 vesicles per active zone (Smith et al. 2008) with the vesicular content extruded in 0.1-100 ms (Travis and Wightman 1998));
- synaptic vesicle molecular content (between 5,000 and 10^6 molecules) (Kandel et al. 1991; Südhof 2004), enumerating the different vesicle pools along with the respective depletion times and refill mechanisms (Rollenhagen and Lübke 2006);
- synaptic vesicle proteic and lipidic composition, typically 40% phosphatidylcholine, 32% phosphatidylethanolamine, 12% phosphatidylserine, 5% phosphatidylinositol, and 10% cholesterol (Südhof 2004);
- the “typical” 20 nm \pm 8 nm synaptic cleft of chemical synapses (Qu et al. 2009);
- fast (~250-400 mm/day), intermediate (~15-50 mm/day), and slow (~0.1-4 mm/day) axonal transport (Perrot et al. 2008); and
- axon growth and axon elimination.

On the borderline between functional and structural monitoring, a controversial question is the importance of monitoring various chemical concentration changes in minimal-size volumetric compartments of, say, 125 nm^3 (5 nm x 5 nm x 5 nm). At this scale, changes are at the most fundamental size limit for computational brain simulation. Neuronanorobots will not monitor every single brain volumetric compartment, but might monitor select volumetric compartments with functional relevance. It remains to be determined how much of this potentially large quantity of structural and functional connectome information is actually essential to enable the computational reconstruction of the human connectome.

3. Recent results in human connectome mapping

The human “connectome” is defined as the full set of human brain neurons and their network of synaptic connections. There is not yet a consensus that the connectome holds the structural correlates of personality and individuality, but it is clear that the human connectome holds valuable human information (Seung 2010). The essential neuronal and synaptic subcomponent building blocks to reconstruct the whole-brain structural and functional connectome remains unknown, but a list of the cellular and molecular components used in computational neural microcircuit connectome reconstruction can be seen elsewhere (Markram, 2006)

Mapping a human whole-brain connectome with cellular and synaptic resolution is the ultimate goal of some current research efforts, and several milestones have already been achieved on the path to solve this grand challenge, as summarized below.

Several small nonhuman brain connectomes have already been preserved computationally, in part or in whole, using destructive and non-destructive techniques.

The first to be mapped, and the best-known publicly, is the *C. elegans* connectome. This effort produced a comprehensive synapse-level nervous system reconstruction using a series of 5000 serial thin (70-90 nm)

sections, including the scanning of the 170 neuron processes and the 64 muscles (White et al. 1986; Chen et al. 2006; Varshney 2011; Jarrell 2012). The online platform “Worm Atlas” contains details on all *C. elegans* systems, including its connectome data (White et al. 1986; WormAtlas 2008; Varshney et al. 2011).

Also scanned and “uploaded” was the connectome of the predatory nematode *Pristionchus pacificus*. The *Pristionchus pacificus* connectome was compared with the *C. elegans* connectome (Bumbarger 2013) and some serious similarities appeared. For example, both the pharyngeal nervous systems of the *Pristionchus pacificus* and the *C. elegans* are composed of a network of 20 identified neurons of 14 cell types. The numeric similarities were associated with differences on the synaptic connectivity mapping of the pharyngeal nervous systems of two nematodes. The differences were proven to be correlated with divergent feeding behavior (Izquierdo and Beer 2013), which can be considered as the first “proof” that brain connectomics information is at least a part of the fundamental structural brain information required for preserving high-level behaviors.

The mouse primary visual cortical connectome (spanning layers 1, 2/3, and upper layer 4) has already been computationally reconstructed, employing a procedure that included structural connectome scanning, using electron microscopy based technology, and functional connectome scanning, using two-photon microscopy to determine the functional properties of about 14 of the cells of that same volume of tissue. This provided a voxel resolution of $45\ \mu\text{m} \times 4\ \mu\text{m} \times 4\ \mu\text{m}$ for a total tissue volume of approximately $450\ \mu\text{m} \times 350\ \mu\text{m} \times 50\ \mu\text{m}$ (Bock et al. 2011).

A structural/functional data project built a neocortical microcircuit database (Ramaswami 2015) with neuron data that included 135 electrophysiological parameters (derived from responses to stimuli), 234 geometric parameters (based on neural reconstruction), and 51 genetic properties (from single cell RT-PCR data). For synapses the data included some physiological properties and 15 parameters for anatomical properties, 5 parameters for synaptic dynamics, and 14 parameters for kinetics.

The inner plexiform layer of the mammalian retina connectome was mapped with $\sim 2\ \text{nm}$ resolution using automated transmission electron microscope imaging, generating a 16.5 terabyte connectome data set. The data represents a column of tissue 0.25 mm in diameter, spanning the inner nuclear, inner plexiform, and ganglion cell layers of the rabbit (Anderson et al. 2011). Data sets from mouse cortex with a $3\ \text{nm} \times 3\ \text{nm} \times 30\ \text{nm}$ spatial resolution had previously yielded 660 gigabytes of images (Kasthuri et al. 2009).

Diffusion imaging (DI) technology, applied on living animals and humans, has permitted mapping long-range projections of small clusters of neurons (without synaptic resolution) (Mori and Zhang 2006; Kasthuri and Lichtman 2007; Bohland et al. 2009; Clayden 2013; Craddock et al. 2013). High-resolution diffusion tensor imaging of the human optic chiasm was performed *ex vivo* at $156\ \mu\text{m}$ resolution in-plane, but the typical DI resolution is on the millimeter range. Whole-brain mesoscale connectomes (i.e. “projectomes”) that are scanned *in vivo* by DI technologies do not contain structural information about individual neuronal cells, and also don’t permit following single axonic processes or identifying individual synapses.

A spinal cord brain map project is close to completion, and the Paul Allen Institute just finished the first phase of a human brain atlas, a four-year project started in 2010 (Allen 2009). A proposed five-year, \$20 million mesoscopic scale mouse connectivity brain map is also underway (Bohland 2009; Modha-blog 2009).

Two-photon calcium imaging combined with large-scale electron microscopy of serial thin sections permits physiological and anatomical reconstruction of a group of neurons in the mouse primary visual cortex (Bock 2011).

Whole brain gene expression information at cellular level – the gene expression map – was computationally reconstructed from histology, with pixel size $0.95\ \mu\text{m}^2$, and from MRI data, voxel size $12.3\ \mu\text{m}^3$ (Lein et al. 2007; Jones 2011; Allen Institute 2014; Allen Institute-mouse 2014).

CLARITY enables estimations of the joint morphological statistics of most neurons in a tissue sample at the same time (Chung 2013; Chung and Deisseroth 2013).

In a project focused on functional data monitoring, detailed system level maps of a human individual’s “functional connectome” were compiled using resting-state functional MRI (R-fMRI) that gathered data from 1,414 brains (Biswal et al. 2010; FCP 2010).

As for achievements at the computational level, daydreaming was simulated by a computational model (Deco et al. 2013). Still at the computational level, IBM claims to have simulated 530 billion neurons and 100 trillion synapses on the world's fastest computer (Theodore et al. 2012).

That is ~ 5 times the number of neurons of a human brain and is very near the total number of synapses of a human brain (est. 2.42×10^{14}) (Martins et al. 2012). It is not clear what they define as a synapse or what the capabilities of those synapses are, but these networks might soon start demonstrating human level subsystem data processing output in limited domains (e.g., visual recognition) using massive parallelization. The computational timescale is ~ 1500 times slower than the human brain timescale (i.e., 1 second of brain time currently takes ~ 25 minutes to simulate) but this doesn't seem to be a problem because most real brain processing/decision happens in seconds (Theodore et al. 2012).

One open source project has the goal of preserving the human connectome with synaptic level resolution (Connectome Project 2011).

The human whole-brain "generic" connectome project has huge implications for Artificial Intelligence and the well-known "Singularity" (e.g., Kurzweil 2005). Two billion-dollar projects are already underway to solve this challenge: the "Human Connectome Project" and the "Brain Research Through Advancing Innovative Neurotechnologies initiative" (BRAIN) (NIH News 2009; Human Brain Project 2013).

The U.S. government called the 1990s the "Decade of the Brain" (Jones and Mendell 1999), but the first serious "call to action" for a coordinated effort to collect, archive, and disseminate the crucial information of the human brain connection matrix was made in 2005 (Sporns et al. 2005; Ascoli 2009). Eight years later, U.S. national agencies launched a formal call for mapping the whole human brain activity map as part of the challenge for functional connectomics (Alivisatos et al. 2012; Kandel et al. 2013).

Destructive structural 3D computational reconstruction of a whole human brain with $20 \mu\text{m}$ resolution (average cellular level resolution) has already been done, nearly preserving the first complete whole human brain neuron soma cytoarchitectural anatomy (Amunts et al. 2013). The next goal was stated to be the creation of a brain model with a spatial voxel resolution of approximately $1 \mu\text{m}$ to capture details of single cell morphology. This is intended to integrate gene expression data from the Allen Institute human brain project. Other projects are taking the effort of mapping the whole human brain connectome with synaptic connections included, and the remaining challenges seem surmountable in the decades ahead (Connectome Project 2011).

Brain tissue structural scanning tools generate tens of petabytes of data for mapping the 1 cm^3 mouse brain with nanometric resolution. As no fully automated tools are currently available, the posterior 3D brain tissue reconstructions currently have to be manually handled (Helmstaedter et al. 2008). In the last 40 years the improvements on the speed of brain scanning and image reconstruction have grown exponentially, and if this trend persists a whole human brain reconstruction should happen in the decades ahead (Kurzweil 2005).

4. Non-destructive vs. destructive scanning techniques

Non-destructive structural whole brain monitoring techniques in the form of computerized scanning-based imaging modalities, such as positron emission tomography (PET) and magnetic resonance imaging (MRI), provide non-destructive three-dimensional views of the brain with $\sim 1 \text{ mm}$ resolution, with clinical MRI scan voxel resolution typically sized $1 \text{ mm} \times 1 \text{ mm} \times 3 \text{ mm}$ (Johnson 2010; Kandel et al. 2000). Such resolution permits regional analyses of brain structure but is clearly insufficient for investigation of structures underlying intercellular communication at the level of individual neurons or synapses (Fiala and Harris 2001). Still at the whole brain level, a non-destructive technique called high-definition fiber tractography provides accurate reconstruction of white matter fiber tracts, but again with a clearly insufficient resolution of $\sim 1 \text{ mm}$ (Shin et al. 2012).

Micro-CT scanners, with a typical scan time between 10 minutes and 2 hours, provide high-resolution tomography of specimens up to a few centimeters in diameter, with the highest spatial resolution being $2 \mu\text{m}$, not enough to detect most synapses. The state-of-the-art tomographic nano-CT scanners (the micro-CT successor) achieves structural resolutions between $500\text{-}50 \text{ nm}$. Currently, there are only three main nano-CT scanners available commercially: the Nanotom, the SkyScan-2011, and the Xradia nanoXCT. The Nanotom provides a resolution of ~ 500 nanometers pixels, and handles maximum object size of 150 mm height and 120 mm diameter (GE-MCS 2013) (roughly the size of a whole human brain). The SkyScan-2011 has a slightly

better resolution of ~400 nm pixels and similar object size constraints. The Xradia nanoXCT claims to be capable of providing a spatial resolution between 300-50 nm (Tkachuk et al. 2007). Although the nano-CT scanner resolutions might permit extraction of some cellular detail and eventually identification of some synapses, a lot of structural information remains un-captured and, most problematically, the technology does not permit *in vivo* brain scanning.

Destructive scanning technologies, by contrast, can achieve near-nanometric structural scanning resolution permitting visualization of individual synapses and their constituents. In a type of destructive brain scanning, an automated ultramicrotome produces large amounts of nanometric 30-100 nm thick sections, which are then scanned by either a transmission electron microscope (TEM) or a serial block-face scanning electron microscopy (SBEM), or by an optical microscope (Hayworth et al. 2006; Anderson and Itallie 2009; Kasthuri et al. 2009; Hayworth 2012). After scanning, posterior software reconstruction uses specialized software, such as RESCOP or KNOSSOS, to trace neuronal connections (Helmstaedter et al. 2011) via individual neuron tagging using fluorescent proteins (aka. brainbow technique), which facilitates the analysis of neuronal circuitry (and mapping of glial territories) on a large scale, and helps on structural cellular level and neuronal circuitry information analysis (Livet et al. 2007; Lichtman et al. 2008). A different high-throughput technique called BOINC (also known as “barcoding of individual neuronal connections”) permits establishing circuit connectivity at single neuron and synaptic resolution using high-throughput DNA sequencing (Zador et al. 2012).

For small size samples, and to avoid the technical difficulties and the laborious process involved in ultrastructural electron microscopy based techniques, X-ray nanotomography with precision down to 30 nm permits avoiding chemically fixation, staining or cutting cells (Helmholtz Association 2010). It can deliver high-resolution 3-D images of the entire fast-frozen cell, but it still takes weeks to be applied in one cell (Helmholtz Association 2010). For single cells, scanning light confocal microscopy provides three-dimensional views of individual neurons down to about 1 μm of resolution.

The current destructive approaches provide near-nanometric atomic structural resolution and seem to be a promising tool for mapping the “generic” whole human brain connectome, provided the speed of scanning a certain brain volume maintains historical improvement rates over the next decades. Although current scanned volumes are far from a whole human brain volume, a process to achieve a whole human brain is envisionable (Hayworth 2012).

There are at least four inherent problems with existing destructive scanning approaches.

First, it is not clear if the different biomolecular machinery can be distinguished by the next generation of these techniques.

Second, although functional information might not be necessary (e.g., if atomic structural resolution were achieved), functional information is not captured by these techniques.

Third, the structural connectome forms the basis for the processing of most functional information that flows in the brain. The interplay between structural and functional information forms the brain as a whole, and although likely, it is unknown if comprehensive structural whole-brain information is sufficient to preserve human life and individuality. Brain simulations are expected to help elucidate the coupling between structural connectivity and functional data, culminating a crucial step to understand the human brain (Friston 2011; Bargmann and Marder 2013).

Fourth, destructive techniques are expected to face resistance from patients during implementation in clinical practice, because the maintenance of consciousness continuity is uncertain or unknown.

In summary, destructive scan technologies are nearer than non-destructive methods to the technical goal of preserving whole human brain connectome information, likely providing enough structural resolution to create at least a static map of a now-disassembled brain. But there are major limitations and serious uncertainties surrounding its applicability in future medical practice with live human patients. Also, while destructive “bottom up” approaches permit nanometric spatial resolution, they cannot easily be applied to whole human brains. For example, electron microscopy permits reconstruction with nanometric resolution, but acquisition rates are too low for the mapping of large volumes (Briggman and Bock 2012).

On the other hand, current non-destructive or “top-down” approaches can scan the whole brain but lack the required spatial resolution. For example, diffusion imaging can image large fiber bundles *in vivo* across the whole brain but the resolution is too coarse to detect single neuronal processes, with DI non-specificity limiting the classification of fiber bundles (Clayden 2013).

The proposed new neuronanorobotics approach appears uniquely to offer whole-brain nanometric scan resolution on a non-destructive basis.

5. Neuronanorobot mission and conceptual design

Neuronanorobotic functional and structural connectome monitoring includes two main tasks: (1) monitoring the *functional* action potential based electrical information processing happening in synapses and neurons; and (2) monitoring the synaptic and neuronal *structural* changes associated with the processing of such electrolytic-based functional data. Two conceptually different approaches can be used to complete these two tasks successfully, with the main difference between strategies residing on the navigation strategy (intracellular navigation or extracellular navigation) and nanorobot positioning strategy (intracellular monitoring or extracellular monitoring). In the proposed mission design, structural and functional connectome monitoring can be done intracellularly using three types of neuronanorobots and an installed *in vivo* fiber optic network (described elsewhere: Freitas 1999). The three types of neuronanorobots – called endoneurobots, gliabots, and synaptobots – are to be stationed, respectively, in the neuron soma, in the glial cells, and near a pre- or post-synaptic side of a synapse (or a set of synapses).

5.1. Rationale for intracellular navigation and monitoring

Multiple considerations appear to favor the choice of intracellular, rather than extracellular, navigation and monitoring by the three different types of neuronanorobots:

(1) Extracellular space is extremely tight, with the average width of the free brain extracellular space (ECS) lying between 38-64 nm (Thorne and Nicholson 2006). ECS width around the cell bodies of oligodendrocytes typically measures 0.3-10 nm; the ECS around the cell bodies of astrocytes oscillates from 4-154 nm. By comparison, a synaptobot is 500 nm in its smallest dimension.

(2) The ECS is thoroughly infiltrated by the extracellular matrix, a structure composed of negatively charged glycosaminoglycans and proteoglycans (Syková 2008) which play a major role in orchestrating the development of the CNS, are involved in remodeling the adult CNS after injury, and are involved in events that may underlie some aspects of memory (Syková 2008). These extracellular space proteins, if seriously disrupted, might cause a cascade of intracellular signaling, triggering neuron epigenetic and structural changes. For example, the application of tension forces to cultured neurons or vascular smooth muscle cells via ECM adhesions results in force-dependent increases in microtubule polymerization (Ingber 2006; Lelièvre 2009).

(3) Each synaptobot might serve between 1-10 synapses, implying a fleet of 24-242 x 10¹² robots to cover the 2.42 x 10¹⁴ synapses in the human brain (Martins et al. 2012) corresponding to a total fleet volume of 1.2-12 x 10¹³ μm³ or 12-120 cm³, representing ~0.9-9% of total human brain volume. This lies within the 1-10% “safe” tissue and organ intrusiveness limit recommended elsewhere (Freitas 2003). If parked extracellularly, this volume of synaptobots would correspond to 4-50% of the extracellular space, likely interfering with, for example, the dynamics of extracellular based-communication, potentially causing considerable neuron epigenetic changes, and potentially causing force-dependent increases in microtubule polymerization. Synaptobots parked intracellularly occupy a much safer fraction of 1.25%-12.5% of the brain intracellular space.

(4) The neuron intracellular environment offers numerous biological proof-of-principle examples of circulating cellular bionanomachinery. Many of these – such as resident mitochondria, synaptic vesicles, and other interior organelles – have similar dimensions to the circulating synaptobots, navigate similar routes, and park in similar regions. Aside from microglia (see below), the extracellular environment is generally reserved for chemical circulation.

(5) Apart from relatively slow neural axon growth, there is no good biological example of large organelles or cells frequently moving around the brain ECS. Extracellular microglia rarely circulate,

are mobilized only after injury, infection, or disease, and are otherwise by default in a resting state. Microglial movements do not represent a massive volume moving in the extracellular space, because microglia constitute only ~20% of the total 85×10^9 glial population in the CNS (Kreutzberg 1995; Azevedo et al. 2009) and are distributed with no significant local differences in the white and grey matter of the brain (Kreutzberg 1995).

(6) Extracellular navigation and monitoring by synaptobots would require a complex communication protocol for establishing a correspondence between neurons and the monitored synapses. With intracellular navigation and monitoring, synapses are by default associated with the appropriate neuron.

We conclude that intracellular navigation and monitoring seem much more appropriate for neuronanorobots. The extracellular space should be used only when intracellular navigation is not possible. This may occur in a few special instances where a small percentage of synaptobots might have to temporarily navigate through the extracellular space to avoid extremely thin axon diameters (Section 5.6).

5.2 Endoneurobots and gliabots

Endoneurobots and gliabots are the larger of the proposed neuronanorobots, each with $10 \mu\text{m}^3$ volume. In their mission, endoneurobots leave the bloodstream to enter the brain parenchyma, and navigate inside the neuropil until they enter the neuron cell soma and get positioned intracellularly in the axon initial segment (AIS). Similarly, gliabots leave the bloodstream, enter the respective glial cell, and position themselves intracellularly in the most appropriate intra-glial region, which varies.

Since action potentials might be initiated in different cellular sub-compartments, endoneurobots will be parked at the AIS (the most likely spot for action potential initiation) where they will monitor the large majority of action potentials. In neurons where some action potentials are initiated at the first nodes of Ranvier or the axon hillock, two synaptobots placed at the first node of Ranvier and at the axon hillock can ensure proper action potential waveform detection.

Endoneurobots monitor action potential based electrical information using FET-based nanosensors existent on the endoneurobot surface (Martins et al. 2015). For monitoring neuronal structural changes (some caused by the processing of action potentials) and once securely anchored to the neuron internal membrane surface ("typical" neurons have a volume of $14,000 \mu\text{m}^3$ or $(\sim 24 \mu\text{m})^3$), endoneurobots might employ a tactile scanning probe to image the surrounding membrane surface area of $(1.4 \text{ micron})^2$ in ~ 2 sec to $\sim 1 \text{ nm}^2$ resolution ($\sim 1 \text{ mm/sec}$ tip velocity), or ~ 50 sec to $\sim 0.2 \text{ nm}$ (e.g., atomic) resolution ($\sim 0.2 \text{ mm/sec}$ tip velocity) assuming a scan rate of $\sim 10^6$ pixels/sec (Freitas 1999). This same scanning tool will be used by all three types of robots.

Endoneurobots and gliabots also provide communication (and data transmission) support for synaptobots.

5.3 Synaptobots

Synaptobots are clearly the most technically challenging of the three neuronanorobots, due to: (1) the small volume of the robots, (2) the navigational requirements necessary to get to the monitoring position, and (3) the challenge of scanning data from synaptic structures. Communication (and data transmission) support is provided by endoneurobots, freeing synaptobots from the necessity of including this high-volume support machinery within their onboard structure.

The task of monitoring raw data traffic for an entire living human brain minimally requires a network data handling capacity of $(5.52 \pm 1.13) \times 10^{16}$ bits/sec, corresponding to an estimated synaptic-processed spike rate of $(4.31 \pm 0.86) \times 10^{15}$ spikes/sec (Martins 2012). This is the event detection requirement for the entire embedded *in vivo* sensor system in the context of nanorobotic whole-brain monitoring. (Non-electrical channels must also be recorded but the data processing requirements for these additional channels are far less demanding; Martins 2012). An *in vivo* nanorobotic auxiliary fiber optic system with 30 cm^3 volume and generating 4-6 watts waste heat (Freitas 1999; Freitas 2010) is capable of handling 10^{18} bits/sec, which enables rapid data transfer (including the action potential waveform) and real-time brain-state monitoring (Freitas 2010; Martins 2012). This auxiliary fiber optic system, coupled with the support for data transmission by endoneurobots and gliabots, minimizes the demand for onboard information storage in synaptobots. The synaptobot nanocomputer might be composed of a $0.01 \mu\text{m}^3$ CPU device capable of >100 megaflops, with 10

onboard copies for redundancy. This is comparable to other nanorobot designs with similar degrees of mission complexity, such as the microbivore with its $0.11 \mu\text{m}^3$ onboard computer and memory storage system (Freitas 2005c).

Synaptobots are the smallest of the three nanorobot types, having a volume of $0.5 \mu\text{m}^3$. Synaptobots are responsible for monitoring synapses, the most challenging and important sub-cellular structures in the human brain. Synapses (either the 5-25% electrical or the 75-95% chemical variety (DeFilipe and Fariñas 1992)) are part of the neural network that processes human brain information. They play a crucial role in brain information processing (IBM 2008) and are involved in learning and memory (Black et al. 1990; Bliss and Collingridge 1993; Holtmaat and Svoboda 2009; Liu 2012), long-term and short-term memory storage and deletion (Kandel 2001; Lee et al. 2008), and temporal information processing (Fuhrmann et al. 2002), and are the key elements for signal transduction and plasticity in the human brain (Rollenhagen and Lübke 2006; Rollenhagen et al. 2007). Synapses are so important that proper synapse formation during childhood provides the substrate for cognition, whereas improper formation or function leads to neuro-developmental disorders, including mental retardation and autism (McAllister 2007). The loss of synapses, as occurs in Alzheimer's patients, is highly related to cognitive decline (Dekosky and Scheff 1990; Terry et al. 1991; Scheff and Price 2006).

In the exemplar synaptobot mission, the robots enter the human body via the bloodstream, later cross the blood-brain barrier to enter the brain parenchyma, and finally enter the respective neuron soma. This process is mediated by the support of auxiliary transport nanorobots.

The synaptobots are delivered via brain vasculature to avoid long-distance navigation inside the brain parenchyma. Auxiliary transport nanorobots of volume $\sim 20 \mu\text{m}^3$ ($\sim 3.2 \times 2.5 \times 2.5 \mu\text{m}$) each convey cargos of 24 synaptobots ($\sim 12 \mu\text{m}^3$) through the circulatory system and into the neuron soma. The full complement of synaptobots are transported by a fleet of ~ 1 trillion auxiliary transport nanorobots, which perform ~ 10 round trips to complete the insertion of all synaptobots in the first medical intervention. Each neuron, on average, receives ~ 117 cargos for an average total delivery of (2.42×10^{14} synapses / 86×10^9 neurons \approx) 2800 synaptobots, assigning one robot per synapse (Martins et al. 2012). The protocol for regularly updating the number of synaptobots in the brain (due to robot damage, synapse elimination, neuron death, new synaptic formation, etc.) is started by the endoneurobots which communicate the necessities. The ~ 1 trillion auxiliary transport nanorobots should suffice to handle the workload of dynamically adjusting the physical deployments of synaptobots.

The protocol that auxiliary transport nanorobots may use to cross the BBB and traverse the neuropil will be similar to the protocol employed by the endoneurobots and the gliabots, due to the similar diameters of auxiliary transport nanorobots ($2.5 \mu\text{m}$) and the endoneurobots and gliabots ($2.2 \mu\text{m}$).

Afterwards, the synaptobots either stay in the neuron soma or navigate from the neuron soma along the axon or dendrite into a pre- or post-synaptic structure. This is the place where synaptic monitoring will occur. To identify the pre- and post-synaptic structures of synapses, synaptobots must necessarily map, from inside the cell, the surfaces of the neuron axon (for axo-axonic, axo-somatic, and axo-dendritic synapses), the soma (for somato-axonic, somato-somatic, or somato-dendritic synapses), and the dendrites (for dendro-somatic, dendro-axonic, and dendro-dendritic synapses). During this process, synaptobots will locate a large variety of synapses in the brain, with the most abundant synapses in the central nervous system being the asymmetric (excitatory) axo-spinous synapses (Harris 1999).

Once at the monitoring position near a pre- or post-synaptic structure, the functional component of the synaptobot mission is to record the exact timing and intensity of the action potential electrical information arriving at the synapses and to monitor the associated changes happening on key structural elements of the synapse. With one synaptobot positioned at each of the 2.42×10^{14} human brain synapses (Martins et al. 2012), action potential data is acquired using $\sim 3375 \text{ nm}^3$ FET-based neuroelectric nanosensors (Martins et al. 2015) permitting monitoring of the synaptic-processed 4.31×10^{15} spikes/sec. Data collection will have a temporal resolution of at least 0.1 ms, which is enough for waveform characterization even at the highest human neuron firing rates of 800 Hz. Assisted by the other two nanorobot types (endoneurobots and gliabots), the synaptobots then transmit the 5.52×10^{16} bits/sec of continuous action potential data (Martins et al. 2012) into the associated *in vivo* fiber optic networking system.

As for the structural component of the synaptobot mission, mapping and subsequent monitoring of relevant neuron structure will be done using tactile scanning probe nanosensors (Freitas 1999) with special scanning tips that permit synaptic bouton volume and shape to be measured, along with other relevant synaptic structural characteristics. An ideal structural scanning process would also permit monitoring the main ultrastructural components of a chemical synapse, whether located in the presynaptic axon terminal, the synaptic cleft, or the post-synaptic terminal. Of primary relevance is the structural information encoded in postsynaptic density (PSD). Other possibly relevant sources of structural information are the active zone (AZ), synaptic vesicles (coated vesicles, dense core vesicles, and double-walled vesicles), endoplasmic reticulum, mitochondria, and punctum adhaerens (PA).

Ideally the tactile nanosensors will permit measurement of:

- (1) the volume, shape, and organelle content of the synaptic boutons.
- (2) the postsynaptic density (PSD) at each synapse, allowing the robot to identify major protein components of the different brain PSDs (comprising up to ~1461 different proteins) (Bayés 2010) with each PSD having on average a total of ~10,000 proteins, typically ~100 copies of ~100 different proteins (Sheng and Hoogenraad 2007).
- (3) the functional information flowing through the “typical” 20 nm \pm 8 nm synaptic cleft of chemical synapses (Qu 2009).

By monitoring synaptic structural changes, the neuronanorobots will also be monitoring synaptic plasticity and cross-talk, including synaptic based long-term potentiation, long-term depression, short-term plasticity, metaplasticity, and homeostatic plasticity.

5.4 Mitochondrial proof of principle

Synaptobots will have an independent locomotion system for moving along axons and dendrites in both directions. While mitochondria depend on an existing neuronal transport system, mitochondria distribution and mobility patterns provide a reasonable biological proof-of-principle of biocompatibility for synaptobots moving along the neuronal processes. Mitochondria and synaptobots are similar in length and volume, with axonal mitochondria existing as discrete organelles typically 1-3 μm in length (Trushina et al. 2012; Sheng 2014), 0.75 μm in diameter, and 0.5 μm^3 in volume (Miyamoto 1986), very close to robot dimensions. The anticipated robot deployment linear number density of ~0.5 synaptobots/ μm -length of axonic or dendritic process is similar to the typical 0.2-0.4 mitochondria/ μm -length in NTG mouse axons (Miyamoto 1986). The deployment volumetric number density of 0.5 synaptobots/ μm^3 of axonic or dendritic process seems acceptable because the more distal dendrites of CA1 hippocampal neurons and the ultrastructural features of synaptic mitochondria indicate a numeric density of 0.8 mitochondria/ μm^3 for mitochondria in the most distal dendrites and in principle the most inaccessible areas of dendrites (Bertoni-Freddari et al. 2006).

The activity levels required for synaptobots are similar to the mobility behaviors exhibited by mitochondria. Synapses have high demand for local mitochondrial ATP production, so the distribution of mitochondria to all neuronal regions requires a bidirectional axonal and dendritic transport system that can deliver and retain these organelles to the appropriate axonal and dendritic regions with high energy requirements (Schwarz 2013). The transport system involves kinesin and dynein motors along with an exceptional number of signaling pathways and regulatory proteins that interact with the dendritic or axonal cytoskeleton. Mitochondria are moved along axons and dendrites bidirectionally over long distances, frequently changing direction, and being stabilized by the actin network. In mature neurons, 10-40% of axonal mitochondria are in motion at any one time – more specifically, 54.07% \pm 2.53% of axonal mitochondria measured in syntaphilin knockout mice are stationary and sitting out of synapses, 16.29 \pm 1.66% are docking at synapses, 14.77 \pm 1.58% are motile and passing through synapses, 7.01 \pm 1.29% are pausing at synapses for short periods of time (<200 s), and 8.30 \pm 1.52% are pausing at synapses for long period of time (>200 s) (Sun et al. 2013).

Synaptobot maximum velocities of ~1 $\mu\text{m}/\text{s}$ are also expected to respect biocompatibility requirements. Bidirectional movements of mitochondria in axons and dendrites are reported at velocities ranging from 0.32-0.91 $\mu\text{m}/\text{s}$ (Morris and Hollenbeck 1995; MacAskill et al. 2009), and mitochondrial motility in NTG neurons is reported as 0.93 \pm 0.55 $\mu\text{m}/\text{sec}$ for anterograde motion and 0.97 \pm 0.63 $\mu\text{m}/\text{sec}$ for retrograde motion (Trushina et al. 2012).

5.5 Nanorobot volumetric intrusiveness in the brain

The “average” human intracranial volume is estimated as 1700 cm³ (Rengachary 2005), being ~1350 cm³ of brain cells (Freitas 1999) (typically with “average” dimensions of ~140 x 167 x 93 mm), ~150 cm³ of blood, and ~150 cm³ of CSF (Rengachary and Ellenbogen 2005). Experimental data provides a considerably wider range for measured intracranial volumes (1152-1839 cm³) and for total average CSF (82-125.3 cm³), with total brain cell parenchyma volume of 1319 cm³ including 489 cm³ of white matter and 786 cm³ of gray matter (Vaidyanathana et al. 1997; Nopoulos et al. 2000). The typical human brain is estimated to have $(86.06 \pm 8.2) \times 10^9$ neurons, with the largest (80.2%) percentage or $(69.03 \pm 6.65) \times 10^9$ neurons located in the cerebellum, the second largest (19%) percentage or $(16.34 \pm 2.17) \times 10^9$ neurons located in the cerebral cortex, and the remaining smallest (0.8%) percentage or $(0.69 \pm 0.12) \times 10^9$ neurons in the rest of the brain (Azevedo et al. 2009).

Inside each neuron will reside one 10 μm³ endoneurobot, a total robot volume of 0.86 cm³ representing ~0.06% of total human brain volume. Parking one 10 μm³ gliabot in each of the $84.6 \pm 9.8 \times 10^9$ glial cells in the human brain (Azevedo et al. 2009) adds another ~0.06% of human brain volume. In each case, the lone nanorobot represents <0.1% of a “typical” ~14,000 μm³ neuron volume, and thus is minimally intrusive.

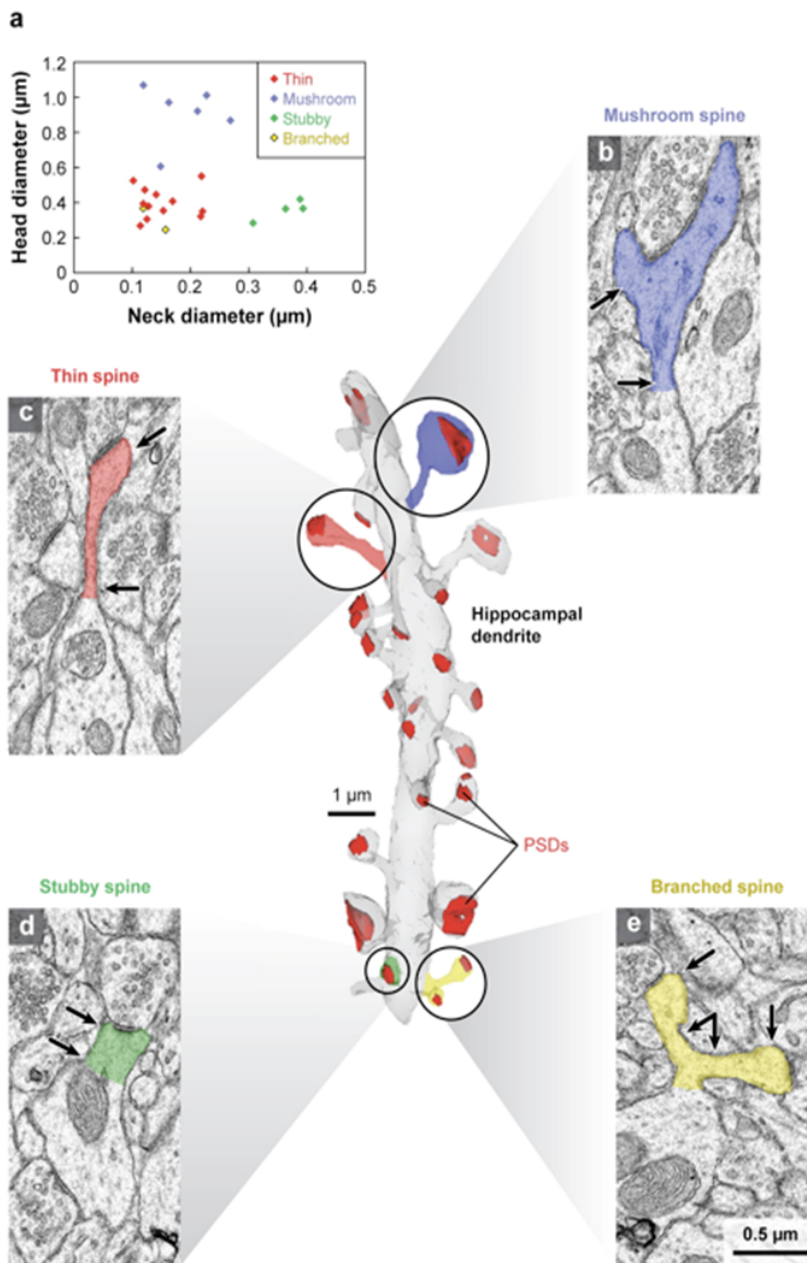
The largest robot intrusion on brain volume occurs with insertion of the synaptobots. How many synaptobots are needed? About 90 per cent of all synapses are in dendritic spines, with “typical” number density of spines ranging from 1-10 spines/μm length of dendrite, depending on neuronal cell type and maturational stage (Calabrese et al. 2006; Sheng and Hoogenraad 2007). For example, the adult mean number of dendritic spines on apical dendrites of pyramidal neurons in layer III of visual cortex is 1 spine/μm, versus 2-4 spines/μm in adult hippocampal CA1 pyramidal and in granule cells, while several Purkinje cells have more than ten spines/μm (Gould et al. 1990; Fiala et al. 1998; Johnson et al. 2002). In these areas with more than one synapse/μm, if each synaptobot possesses ten neuroelectrical nanosensors (est. 3375 nm³ each (Martins et al. 2015)) then a single robot can monitor action potentials on up to ten different synapses with adequate temporal resolution. Assuming 2.42×10^{14} synapses in the human brain (Martins et al. 2012) and with each synaptobot servicing 1-10 synapses, the required number of 0.5 μm³ synaptobots is 24-242 x 10¹² robots having total fleet volume of 1.2-12 x 10¹³ μm³ or 12-120 cm³, representing ~0.9-9% of total human brain volume. This lies within the 1-10% “safe” tissue and organ intrusiveness limit recommended elsewhere (Freitas 2003).

5.6 Special nanorobot designs and protocols

Special nanorobot designs and operational protocols may be required for areas in which intracellular navigation is seriously constrained. Axon and dendritic regions with less than 0.50 μm of diameter are the most serious example (Shepherd and Harris 2010). The diameter of axons within the mammalian nervous system had been reported to vary by a factor of more than 100 (Liewald 2014), but closer study of the frequency distribution of the diameters of myelinated axons in three different locations of the corpus callosum in human brains suggested that 70-90 per cent of axon diameters are ≥0.50 μm, with minimum and maximum diameters of 0.16 μm and 3.73 μm respectively, and a mean value and standard deviation of 0.73 ± 0.55 μm (Liewald et al. 2014). A small percentage of 0.5 μm³ synaptobots might have difficulty intracellularly reaching the most distal axonic and dendritic regions, depending on nanorobot shape.

Special robot-form factor design choices will be required for scanning structural information inside some of the longest and thinnest dendritic spines. The postsynaptic structure of 90 per cent of the excitatory synapses in the mammalian brain are dendritic spines (Sheng and Hoogenraad 2007; Bhatt et al. 2009). These are functionally important because they can compartmentalize calcium and serve a myriad of functions ranging from basic computational operations to synaptic plasticity based on coincidence (Contreras 2004). Learning-associated structural changes involve various synaptic changes including: (1) formation of new dendritic spines, (2) changes in shape and size of existing dendritic spines, and (3) changes in the organization of postsynaptic densities of spines (De Roo et al. 2008). Spine shapes (Figure 1) are commonly categorized as “mushroom” (~60% of all spines in adult cortex), “thin” (10-20%), “stubby” (20-25%), “filopodia” (2-15%), and “branched” (a small number), with a continuum among these categories (Sheng and Hoogenraad 2007). Across all types, ~0.5-2 μm diameter spine heads (Sheng and Hoogenraad 2007; Sala et al. 2008) connect to the dendrite through 0.04-1 μm long necks (Calabrese et al. 2006). Most spines are located on dendrites but some may also be present on the soma or the axonal initial segment, and some spines receive more than one synapse, e.g., the branched type (Spacek 2006).

Figure 1. Three dimensional reconstruction of a hippocampal dendrite.



Three dimensional reconstruction of a hippocampal dendrite (gray) (from Area CA1 of the Rat) illustrate the four main types of different spine shapes, including mushroom (blue)(b), thin (red)(c), stubby (green)(d), and branched (yellow)(e). PSDs (red) also vary in size and shape. On (a) a graph plots the ratio of head diameters to neck diameters for the spines on the reconstructed dendrite. Arrows indicate where the head and neck diameters were measured for each spine in b–e. Scale bar = 0.5 µm. (Reprinted with Permission)(from (Bourne and Harris 2008)).

Synaptobots should readily fulfill temporal resolution requirements for monitoring gross changes in spine structure. Spine lifetimes vary greatly – stable ones may persist for at least a month, whereas others may last for a few days or less (Trachtenberg 2002) – but spine shape can change over periods of minutes or hours (Sala et al. 2008). Synaptobots should be able to distinguish pre-spinal filopodia processes from regular synapses because filopodia have turnover times measured in hours, with only ~20% of filopodia turning into spines and 80% disappearing within 48 h (Alvarez and Sabatini 2007; Zuo et al. 2005).

Unilaterally positioning sensors at either the pre- or the post-synaptic side of axo-spinous, dendro-spinous, or soma-spinous synapses may be sufficient. (Spino-spinous synapses, where two spines directly contact, are rare.) However, for redundancy purposes it might be desirable for neuronanorobots to position sensors on both synaptic sides. Such bilateral monitoring might be challenging depending on spine morphology, diameter, and

neck lengths. In especially narrow cases, the mission design can include insertion of a nanomanipulator from the opposite side.

Spine monitoring includes not only volume and shape tracking but may also include local organelle scanning when necessary. Spines typically have organelles inside or near the entrance, including the smooth endoplasmic reticulum, spine apparatus, actin cytoskeleton, endosomal compartments, translation machinery components (e.g., polyribosomes), and the crucial postsynaptic density (PSD) which occupies ~10 per cent of the surface area and is opposite to the presynaptic active zone (Sheng and Hoogenraad 2007; Sala et al. 2008). Synaptic plasticity is mediated by changes in the molecular composition of synaptic proteins (Sheng and Hoogenraad 2007), and many of those proteins are located in the PSD, a structure composed of ~1461 membranous and cytoplasmic proteins (Bayés 2010) localized at the postsynaptic plasma membrane of excitatory synapses (Figure 2).

Figure 2: The variety of proteins in the PSD fraction.

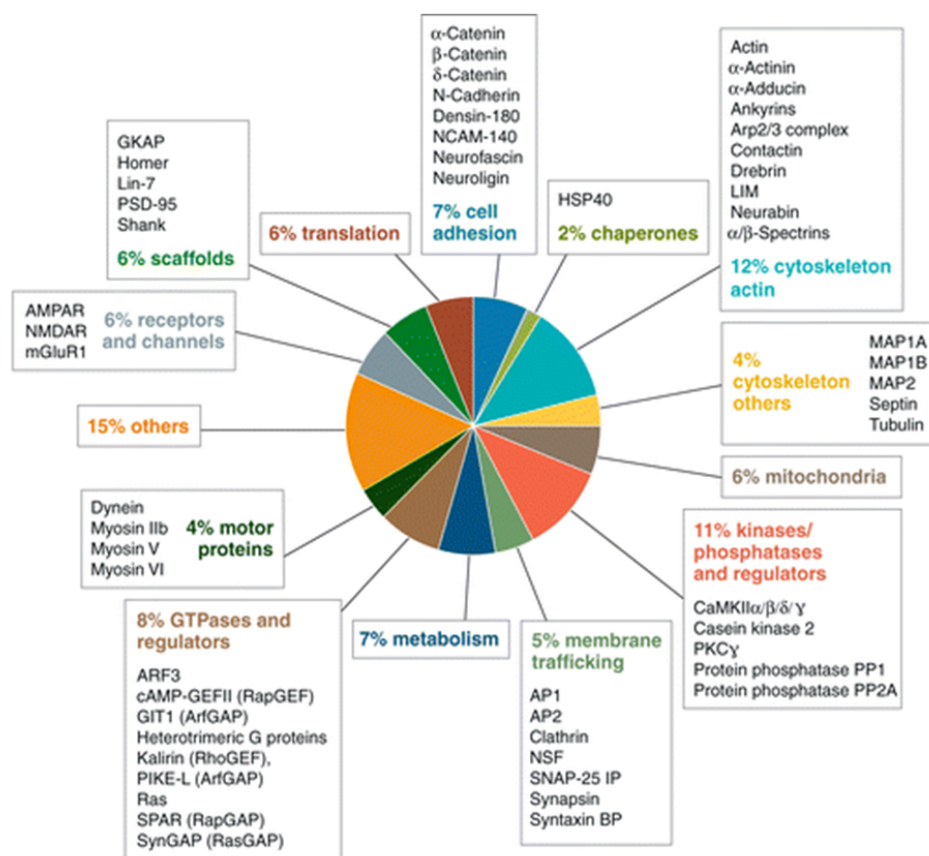


Illustration of some of the variety of proteins on PSD (categorized according to cellular function). Only small subsets of identified proteins are shown as examples (Reprinted with Permission)(from (Sheng and Hoogenraad 2007)).

Nanorobotic monitoring of the PSD seems essential. The PSD is a complex molecular machine that dynamically changes its structure and composition in response to synaptic activity, which dynamically regulates its components through protein phosphorylation, palmitoylation, local protein translation, the ubiquitin-proteasome system for protein degradation, and redistribution of specific proteins, such as CaMKII α and AMPARs, both to and away from the PSD (Kim and Ko 2006; Sheng and Hoogenraad 2007). PSD proteins organize signaling pathways to coordinate structural and functional changes in synapses. The PSD regulates trafficking and recycling of glutamate receptors (which determines synaptic strength and plasticity), promotes the formation and maturation of excitatory synapses by co-aggregating with post-synaptic cell adhesion molecules, organizes neurotransmitter receptors in the synaptic cleft, serves as a signaling apparatus, and is an essential component of an extraordinary synaptic signaling assemblage that has a strong relation with important mechanisms for synaptic regulation, including long-term potentiation (LTP) and long-term depression (LTD) (Sheng and Hoogenraad 2007).

The structure and composition of the PSD is modified by external stimuli and by synaptic activity over the time course of seconds to minutes and hours to days (Sheng and Hoogenraad 2007). The “typical” PSD is a disklike structure with an average diameter of 300-400 nm diameter (range 200-800 nm), a thickness of 30-60 nm (Baude et al. 1993; Rácz et al. 2004; Okabe 2007; Sheng and Hoogenraad 2007), estimated volume $7.5 \times 10^6 \text{ nm}^3$ and mass $\sim 1.1 \text{ GDa}$ (Chen et al. 2005).

5.7 Measuring synaptic plasticity

Nanorobots can directly measure changes in synaptic plasticity. For instance, the activity-dependent modification of PSD proteins over a timescale of seconds to hours is believed to underlie plasticity processes such as LTP and LTD (Sheng and Hoogenraad 2007). Longer-term changes in PSD structure and composition (hours to days) involve altered protein synthesis, either in the neuronal cell body or dendrites (Sheng and Hoogenraad 2007). Degradation of PSD proteins by the ubiquitin-proteasome system (Bingol and Schuman 2006) sculpts PSD structure and plays a major role in synaptic plasticity. Remarkably, recent evidence even points toward a rapid exchange of PSD proteins, such as AMPARs and PSD-95, between neighboring synapses in steady-state conditions (Sheng and Hoogenraad 2007).

LTP and LTD events cause structural changes to spines, altering spine number, size, shape, and subcellular composition in both immature and mature spines (Bourne and Harris 2008). The spine neck acts as a diffusion barrier (controlled by neuronal activity) to current flow and to the diffusion of molecules between the spine head and the dendrite. The geometry of the spine neck determines calcium efflux into the dendrite shaft and hence the degree of calcium elevation in the spine head following NMDAR activation (Bloodgood and Sabatini 2005; Sheng and Hoogenraad 2007; Alvarez and Sabatini 2007).

In experimental work, spines that received LTP induction increased in volume from 50-200 per cent (Alvarez and Sabatini 2007) with the increase persisting for more than 1 hour after stimulation (Alvarez and Sabatini 2007). LTP causes sustained spine head enlargement due to F-actin polymerization, while LTD causes AMPA receptor internalization with spine elongation and/or shrinkage of spine heads due to actin depolymerization (Bourne and Harris 2008). More detailed synaptic structural changes (within synaptic plasticity limits) occur in the:

- (1) size and composition of the postsynaptic density;
- (2) assembly and disassembly of actin filaments;
- (3) exocytosis and endocytosis of glutamate receptors and ion channels;
- (4) regulation of local protein synthesis by redistribution of polyribosomes and proteasomes;
- (5) dynamic repositioning of smooth endoplasmic reticulum (SER) and mitochondria; and
- (6) metabolic and structural interactions between spines and perisynaptic astroglia (Bourne and Harris 2008).

There is a clear strong relation between synapse bouton size and shape, and the organelle and macromolecular changes happening inside synapses. This provides some level of redundancy of information, which suggests that monitoring all the spine organelles and molecular components is very likely unnecessary. Synaptobots can deduce a great deal of useful information when they scan the gross volume and shape of the spine. The redundancy of information is expected to seriously reduce the monitoring tasks of the synaptobots. However, to quantify and identify what information is deducible from where will require more data on the range of quantitative ultrastructural synaptic characteristics found throughout the different brain areas. Details of the quantitative morphology of synapses are still limited to a relatively small number of synapses (Rollenhagen and Lübke 2006), which points to the need for further experimental data.

6. Conclusions

Fundamental, life-saving, structural and functional human connectome-associated information cannot be preserved using current destructive or non-destructive human brain imaging technologies. Those technologies, as an extension of current form, seem not to be theoretically scalable to the desired level of temporal or spatial resolution required to preserve human cognitive life. Non-destructive preservation of comprehensive *in vivo* whole-human brain information is proposed to be achieved using a set of neuronanorobots, named endoneurobots, gliabots, and synaptobots, conceptually designed in this paper. Such nanorobots should

preserve the underlying structural and functional information of the human brain with appropriate temporal and spatial resolution.

Acknowledgments

The principal author (NRBM) thanks the Fundação para a Ciência e Tecnologia (FCT) for their financial support of this work (grant SFRH/BD/69660/2010). The author also thanks for the support granted by Qualificar é Crescer, Quadro de Referência Estratégico Nacional, União Europeia Fundo Social Europeu, and Governo da República Portuguesa.



Glossary of terms and abbreviations

Field-effect transistor (FET) is a transistor using an electric field to control the electrical conductivity of a channel in a semiconductor material.

Micro computed tomography (Micro-CT) uses x-rays to non-destructively create cross-section images of a certain physical object for later 3D reconstruction.

Axon initial segment (AIS) is a specific axonic membrane region with specific clusters of voltage-gated channels where action potentials are frequently initiated.

The postsynaptic density (PSD) is a specific membrane region of a postsynaptic neuron (in close apposition to the presynaptic active zone) being particularly dense in proteins.

Magnetic resonance imaging (MRI) is a widely used medical imaging technique using magnetic fields and radio waves to permit 3D anatomical and physiological reconstructions of parts of the human body.

Functional magnetic resonance imaging (fMRI) is a neuro-imaging technique for measuring brain activity by detecting blood flow associated changes.

Resting state fMRI (R-fMRI) is a method for functional brain imaging of the resting brain activity by detecting blood-oxygen-level dependent signals measurable using functional magnetic resonance imaging.

Electron microscope (EM) is a microscope using beams of accelerated electrons as its illumination source typically providing higher resolution than light microscopy.

Serial block-face scanning electron microscopy (SBEM) is a method for 3D ultra high-resolution imaging using an ultramicrotome mounted inside a vacuum chamber of a scanning electron microscope.

Transmission electron microscope (TEM) is a microscope using beams of electrons transmitted through an ultra-thin specimen and focused onto a sensorial layer, screen or device.

References

Alivisatos, A.P., M. Chun, G.M. Church, R.J. Greenspan, M.L. Roukes, and R. Yuste. 2012. The Brain Activity Map Project and the challenge of functional connectomics. *Neuron* 74(6): 970–74.

Allen, P. 2009. Piece of mind, the world in 2009. *The Economist*.

Allen Institute for Brain Science. 2014. Allen Brain Atlas. <http://human.brain-map.org/> (accessed December 23, 2015).

Allen Institute for Brain Science. 2014. Allen Institute for Brain Science. Allen Mouse Brain Atlas.

<http://mouse.brain-map.org/> (accessed December 23, 2015).

Alvarez, V.A., and B.L. Sabatini. 2007. Anatomical and physiological plasticity of dendritic spines. *Annual Reviews of Neuroscience* 30: 79–97.

Amunts, K., C. Lepage, L. Borgeat, H. Mohlberg, T. Dickscheid, M. Rousseau, S. Bludau, P. Bazin, L.B. Lewis, A. Oros-Peusquens, N.J. Shah, T. Lippert, K. Zilles, and A.C. Evans. 2013. BigBrain: An ultrahigh-resolution 3D human brain model. *Science* 21 June. Vol. 340 no. 6139: 1472-1475.

Anderson, J., and C.M.V. Itallie. 2009. Physiology and function of the tight junction. *Cold Spring Harbor Perspectives in Biology* 1(2): a002584.

Anderson, J.R., B.W. Jones, C.B. Watt, M.V. Shaw, J.H. Yang, D. Demill, J.S. Lauritzen, Y. Lin, K.D. Rapp, D. Mastronarde, P. Koshevoy, B. Grimm, T. Tasdizen, R. Whitaker, and R.E. Marc. 2011. Exploring the retinal connectome. *Molecular Vision* 17: 355–65.

Arking, R. 2006. *Biology of aging: Observations and principles*. 3rd ed. New York: Oxford University Press.

Ascoli, G. 2009. Coming of age of the hippocampome. *Front. Neur. Conference Abstract: Neuroinformatics 2009*.

Astier, Y., H. Bayley, and S. Howorka. 2005. Protein components for nanodevices. *Current Opinion in Chemical Biology* 9(6): 576–84.

Azevedo, F.A., L.R. Carvalho, L.T. Grinberg, J.M. Farfel, R.E. Ferretti, R.E. Leite, W.J. Filho, R. Lent, and S. Herculano-Houzel. 2009. Equal numbers of neuronal and nonneuronal cells make the human brain an isometrically scaled-up primate brain. *Journal of Comparative Neurology* 513(5): 532–41.

Baude, A., Z. Nusser, J.D. Roberts, E. Mulvihill, R.A. McIlhinney, and P. Somogyi. 1993. The metabotropic glutamate receptor (mGluR1 alpha) is concentrated at perisynaptic membrane of neuronal subpopulations as detected by immunogold reaction. *Neuron* 11(4): 771–87.

Bargmann, C.I., and E. Marder. 2013. From the connectome to brain function. *Nature Methods* 10: 483–90.

Bayés, A. 2010. Characterization of the proteome, diseases and evolution of the human postsynaptic density. *Nature Neuroscience* 14(1): 19–21.

Bertoni-Freddari, C., P. Fattoretti, T. Casoli, G. Di Stefano, M. Solazzi, E. Perna, and C. Angelis. 2006. Reactive structural dynamics of synaptic mitochondria in ischemic delayed neuronal death. *Annals of the New York Academy of Sciences* 1090(1): 26–34.

Bhatt, D.H., S. Zhang, and W-B. Gan. 2009. Dendritic spine dynamics. *Annual Review of Physiology* 71: 261–82.

Bingol, B., and E.M. Schuman. 2006. Activity-dependent dynamics and sequestration of proteasomes in dendritic spines. *Nature* 441: 1144–1148.

Biswal, B.B., M. Mennes, X-N. Zuo, S. Gohel, C. Kelly, S.M. Smith, C.F. Beckmann, J.S. Adelstein, R.L. Buckner, S. Colcombe, A-M. Dogonowski, M. Ernst, D. Fair, M. Hampson, M.J. Hoptman, J.S. Hyde, V.J. Kiviniemi, R. Kötter, S-J. Li, C-P- Lin, M.J. Lowe, C. Mackay, D.J. Madden, K.H. Madsen, D.S. Margulies, H.S. Mayberg, K. McMahon, C.S. Monk, S.H. Mostofsky, B.J. Nagel, J.J. Pekar, S.J. Peltier, S.E. Petersen, V. Riedl, S.A.R.B. Rombouts, B. Rypma, B.L. Schlaggar, S. Schmidt, R.D. Seidler, G.J. Siegle, C. Sorg, G-J. Teng, J. Veijola, A. Villringer, M. Walter, L. Wang, X-C. Weng, S. Whitfield-Gabrieli, P. Williamson, C. Windischberger, Y-F. Zang, H-Y. Zhang, F.X. Castellanos, and M.P. Milham. 2010. Toward discovery science of human brain function. *Proceedings of the National Academy of Sciences* 107(10): 4734–4740.

- Black, J.E., K.R. Isaacs, B.J. Anderson, A.A. Alcantara, and W.T. Greenough. 1990. Learning causes synaptogenesis, whereas motor activity causes angiogenesis, in cerebellar cortex of adult rats. *Proceedings of the National Academy of Sciences* 87: 5568–5572.
- Bliss, T.V.P., and G.L. Collingridge. 1993. A synaptic model of memory: Long-term potentiation in the hippocampus. *Nature* 361: 31–39.
- Bloodgood, B.L., and B.L. Sabatini. 2005. Neuronal activity regulates diffusion across the neck of dendritic spines. *Science* 4: 866–69.
- Bock, D.D., W-C.A. Lee, A.M. Kerlin, M.L. Andermann, G. Hood, A.W. Wetzel, S. Yurgenson, E.R. Soucy, H.S. Kim, and R.C. Reid. 2011. Network anatomy and *in vivo* physiology of visual cortical neurons. *Nature* 471: 177–82.
- Bohland, C.W., H. Barbas, H. Bokil, M. Bota, H.C. Breiter, H.T. Cline, J.C. Doyle, P.J. Freed, R.J. Greenspan, S.N. Haber, M. Hawrylycz, D.G. Herrera, C.C. Hilgetag, Z.J. Huang, A. Jones, E.G. Jones, H.J. Karten, D. Kleinfeld, R. Kötter, H.A. Lester, J.M. Lin, B.D. Mensh, S. Mikula, J. Panksepp, J.L. Price, J. Safdieh, C.B. Saper, N.D. Schiff, J.D. Schmahmann, B.W. Stillman, K. Svoboda, L.W. Swanson, A.W. Toga, D.C. Van Essen, J.D. Watson, and P.P. Mitra. 2009. A proposal for a coordinated effort for the determination of brainwide neuroanatomical connectivity in model organisms at a mesoscopic scale. *PLoS Computational Biology* 5(3): e1000334.
- Bourne, J.N., and K.M. Harris. 2008. Balancing structure and function at hippocampal dendritic spines. *Annual Review of Neuroscience* 31: 47–67.
- Briggman, K.L., and D.D. Bock. 2012. Volume electron microscopy for neuronal circuit reconstruction. *Current Opinion in Neurobiology* 22: 154–61.
- Bumbarger, D. J., M. Riebesell, C. Rödelberger, and R.J. Sommer. 2013. System-wide rewiring underlies behavioral differences in predatory and bacterial-feeding nematodes. *Cell* 152(1): 109–119.
- Calabrese B., M.S. Wilson, and S. Halpain. 2006. Development and regulation of dendritic spine synapses. *Physiology* 21(1): 38–47.
- Chen, X., L. Vinade, R.D. Leapman, J.D. Petersen, T. Nakagawa, T.M. Phillips, M. Sheng, and T.S. Reese. 2005. Mass of the postsynaptic density and enumeration of three key molecules. *Proceedings of the National Academy of Sciences* 102: 11551–11556.
- Chen, B.L., D.H. Hall, and D.B. Chklovskii. 2006. Wiring optimization can relate neuronal structure and function. *Proceedings of the National Academy of Sciences* 103: 4723–4728.
- Chung, K. 2013. Structural and molecular interrogation of intact biological systems. *Nature* 497: 332–37.
- Chung, K., and K. Deisseroth. 2013. CLARITY for mapping the nervous system. *Nature Methods* 10(6): 508–13.
- Clayden, J.D. 2013. Imaging connectivity: MRI and the structural networks of the brain. *Functional Neurology* 28: 197–203.
- Connectome Project. 2011. Open connectome project: Collectively reverse engineering the brain, one synapse at a time.
<http://www.openconnectomeproject.org> (accessed December 23, 2015).
- Contreras, D. 2004. Electrophysiological classes of neocortical neurons. *Neural Networks* 17(5–6): 633–46.

- Craddock, R.C., S. Jbabdi, C.G. Yan, J.T. Vogelstein, F.X. Castellanos, A. Di Martino, C. Kelly, K. Heberlein, S. Colcombe, and M.P. Milham. 2013. Imaging human connectomes at the macroscale. *Nature Methods* 10: 524–39.
- De Roo, M., P. Klauser, P.M. Garcia, L. Poggia, and D. Muller. 2008. Spine dynamics and synapse remodeling during LTP and memory processes. *Progress in Brain Research* 169: 199–207.
- Deco, G., A. Ponce-Alvarez, D. Mantini, G.L. Romani, P. Hagmann, and M. Corbetta. 2013. Resting-state functional connectivity emerges from structurally and dynamically shaped slow linear fluctuations. *Journal of Neuroscience* 33(27): 11239–11252.
- DeFelipe, J., and I. Fariñas. 1992. The pyramidal neuron of the cerebral cortex: Morphological and chemical characteristics of the synaptic inputs. *Progress in Neurobiology* 39: 563–607.
- Dekosky, S.T., and S. Scheff. 1990. Synapse loss in frontal cortex biopsies in Alzheimer’s disease: correlation with cognitive severity. *Annals of Neurology* 27(5): 457–64.
- Donohue, D.E., and G.A. Ascoli. 2008. A comparative computer simulation of dendritic morphology. *PLoS Computational Biology* 4(6): e1000089.
- FCP. 2010. 1000 Functional Connectomes Project. http://fcon_1000.projects.nitrc.org/fcpClassic/FcpTable.html (accessed January 5, 2196).
- Fiala, J.C., M. Feinberg, V. Popov, and K.M. Harris. 1998. Synaptogenesis via dendritic filopodia in developing hippocampal area CA1. *Journal of Neuroscience* 18: 8900–8911.
- Fiala, J.C., and K.M. Harris. 2001. Extending unbiased stereology of brain ultrastructure to three-dimensional volumes. *Journal of the American Medical Informatics Association* 8(1): 1–16.
- Freitas, R.A., Jr. 1999. *Nanomedicine. Volume I: Basic capabilities*. Georgetown, TX: Landes Bioscience.
- Freitas, R.A., Jr. 2000. Nanodentistry. *Journal of the American Dental Association* 131: 1559–1566.
- Freitas, R.A., Jr. 2003. *Nanomedicine. Volume IIA: Biocompatibility*. Georgetown, TX: Landes Bioscience.
- Freitas, R.A., Jr. 2005a. What is nanomedicine? *Disease-A-Month* 51: 325–41.
- Freitas, R.A., Jr. 2005b. Current status of nanomedicine and medical nanorobotics. *Journal of Computational and Theoretical Nanoscience* 2: 1–25.
- Freitas, R.A., Jr. 2005c. Microbivores: Artificial mechanical phagocytes using digest and discharge protocol. *Journal of Evolution and Technology* 14 (April): 1–52. Available online <http://jetpress.org/volume14/freitas.pdf> (accessed December 23, 2015).
- Freitas, R.A., Jr. 2006a. Pharmacytes: An ideal vehicle for targeted drug delivery. *Journal of Nanoscience and Nanotechnology* 6: 2769–2775.
- Freitas, R.A., Jr. 2006b. Progress in nanomedicine and medical nanorobotics. In *Handbook of theoretical and computational nanotechnology. Volume 6: Bioinformatics, nanomedicine, and drug design*, ed. M. Rieth, and W. Schommers, 619–72. Stevenson Ranch, CA: American Scientific Publishers.
- Freitas, R.A., Jr. 2007. The ideal gene delivery vector: Chromalloytes, cell repair nanorobots for chromosome replacement therapy. *Journal of Evolution and Technology* 16 (June): 1–97. Available online <http://jetpress.org/v16/freitas.pdf> (accessed December 23, 2015).

- Freitas, R.A., Jr. 2010. Comprehensive nanorobotic control of human morbidity and aging. In *The future of aging: Pathways to human life extension*, ed. G.M. Fahy, M.D. West, L.S. Coles, and S.B. Harris, 685–805. New York: Springer.
- Friston, K.J. 2011. Functional and effective connectivity: A review. *Brain Connectivity* 1: 13–36.
- Fuhrmann, G., I. Segev, H. Markram, and M. Tsodyks. 2002. Coding of temporal information by activity-dependent synapses. *Journal of Neurophysiology* 87(1): 140–48.
- GE-MCS. 2013. Phoenix Nanotom M.
<http://www.ge-mcs.com/en/radiography-x-ray/ct-computed-tomography/nanotom-s.html>
or
https://www.gemeasurement.com/sites/gemc.dev/files/nanotom_brochure_english_0.pdf (accessed December 23, 2015).
- Gross, C.G. 2000. Neurogenesis in the adult brain: Death of a dogma. *Nature Reviews Neuroscience* 1: 67–73.
- Gould, E., C.S. Woolley, M. Frankfurt, and B.S. McEwen. 1990. Gonadal steroids regulate dendritic spine density in hippocampal pyramidal cells in adulthood. *Journal of Neuroscience* 10: 1286–1291.
- Harris, K. M. 1999. Synapse Web.
<http://synapses.clm.utexas.edu> (accessed December 23, 2015).
- Hayworth, K.J., N. Kasthuri, R. Schalek, and J.W. Lichtman. 2006. Automating the collection of ultrathin serial sections for large volume TEM reconstructions. *Microscopy and Microanalysis* 12(Suppl 2): 86–87.
- Hayworth, K.J. (2012) Electron imaging technology for whole brain neural circuit mapping. *International Journal of Machine Consciousness* 4(1) 87–108.
- Helmholtz Association. 2010. New microscope reveals ultrastructure of cells. Public release: Nov 19.
- Helmstaedter, M., K.L. Briggman, and W. Denk. 2008. 3D structural imaging of the brain with photons and electrons. *Current Opinion in Neurobiology* 18: 633–41.
- Helmstaedter, M., K.L. Briggman, and W. Denk. 2011. High-accuracy neurite reconstruction for high-throughput neuroanatomy. *Nature Neuroscience* 14: 1081–1088.
- Herculano-Houzel, S. 2009. The human brain in numbers: A linearly scaled-up primate brain. *Frontiers in Human Neuroscience* 9(3): 31.
- Holtmaat, A., and K. Svoboda. 2009. Experience-dependent structural synaptic plasticity in the mammalian brain. *Nature Reviews Neuroscience* 10: 647–658.
- Human Brain Project. 2013. Human Brain Project.
<https://www.humanbrainproject.eu> (accessed January 5, 2016).
- IBM. 2008. IBM seeks to build the computer of the future based on insights from the brain – IBM awarded DARPA funding for cognitive computing collaboration.
<https://www-03.ibm.com/press/us/en/pressrelease/26123.wss> (accessed December 23, 2015).
- IHGSC. 2004. International Human Genome Sequencing Consortium: Finishing the euchromatic sequence of the human genome. *Nature* 431: 931–45.
- Ingber, D.E. 2006. Cellular mechanotransduction: Putting all the pieces together again. *Journal of the Federation of American Societies for Experimental Biologies (FASEB)* 20(7): 811–27.

- Islam, S. 2011. Characterization of the single-cell transcriptional landscape by highly multiplex RNA-seq. *Genome Research* 21: 1160–1167.
- Izquierdo, E.J., and R.D. Beer 2013. Connecting a connectome to behavior: An ensemble of neuroanatomical models of *C. elegans* klinotaxis. *PLoS Computational Biology* 9(2): e1002890.
- Johnson, G.A. 2010. An image-based reference for coordinating mouse brain research. *NeuroImage* 53(2): 365.
- Johnson, M.H., Y. Munakata, and R. Gilmore. 2002. *Brain development and cognition: A reader*. 2nd Edition. Oxford: Blackwell.
- Jones, A. 2011. Allen Institute: A map of the brain, TED Global Talk. Weblink: https://www.ted.com/talks/allan_jones_a_map_of_the_brain?language=en (accessed December 23, 2015)
- Jones, E.G., and L.M. Mendell. 1999. Assessing the decade of the brain. *Science* 284(5415): 739.
- Kandel, E.R., J. Schwartz, and T. Jessell. 1991. *Principles of neural science*. 3rd ed. New York: McGraw-Hill.
- Kandel, E.R. 2001. The molecular biology of memory storage: A dialogue between gene and synapses. *Science* 294 (5544): 1030–1038.
- Kandel, E.R., J. Schwartz, and T. Jessell. 2000. *Principles of neural science*. 4th ed. New York: McGraw Hill.
- Kandel, E.R., H. Markram, P.M. Matthews, R. Yuste, and C. Koch. 2013. Neuroscience thinks big (and collaboratively). *Nature Reviews Neuroscience* 14: 659–64.
- Kasthuri, N., K. Hayworth, J.C. Tapia, R. Schalek, S. Nundy, and J.W. Lichtman. 2009. Thin section scanning electron microscopy of serial sections of brain on tape. *Neuroscience Meeting Planner*. Chicago, IL: Society for Neuroscience, 2009.
- Kasthuri, N., and J.W. Lichtman. 2007. The rise of the “projectome.” *Nature Methods* 4(4): 307–308.
- Kim, E., and J. Ko. 2006. Molecular organization and assembly of the postsynaptic density of excitatory brain synapses. *Results and Problems in Cell Differentiation* 43: 1–23.
- Kleinfeld, D., A. Bharioke, P. Blinder, D.D. Bock, K.L. Briggman, D.B. Chklovskii, W. Denk, M. Helmstaedter, J.P. Kaufhold, W-C. A. Lee, H.S. Meyer, K.D. Micheva, M. Oberlaender, S. Prohaska, R.C. Reid, S.J. Smith, S. Takemura, P.S. Tsai, and B. Sakmann. 2011. Large-scale automated histology in the pursuit of connectomes. *Journal of Neuroscience* 31(45): 16, 125–16, 138.
- Kole, M.H. P., J.J. Letzkus, and G.J. Stuart. 2007. Axon initial segment Kv1 channels control axonal action potential waveform and synaptic efficacy. *Neuron* 55(4): 633–47.
- Kostarelos K. 2010. Nanorobots for medicine: How close are we? *Nanomedicine* 5(3): 341–42.
- Kreutzberg, G. W. 1995. The first line of defense in brain pathologies. *Drug Research* 45(1): 357–60.
- Kurzweil, R. 2005. *The Singularity is near*. New York: Viking.
- Lee, S.H., J.H. Choi, N. Lee, H.R. Lee, J.L. Kim, N.K. Yu, S.L. Choi, S.H. Lee, H. Kim, and B.K. Kaang. 2008. Synaptic protein degradation underlies destabilization of retrieved fear memory. *Science* 319(5867): 1253–1256.
- Lein, E.S., M.J. Hawrylycz, N. Ao, M. Ayres, A. Bensinger, A. Bernard, A.F. Boe, M.S. Boguski, K.S. Brockway, E.J. Byrnes, L. Chen, L. Chen, T-M. Chen, M.C. Chin, J. Chong, B.E. Crook, A. Czaplinska, C.N.

Dang, S. Datta, N.R. Dee, A.L. Desaki, T. Desta, E. Diep, T.A. Dolbeare, M.J. Donelan, H-W. Dong, J.G. Dougherty, B.J. Duncan, A.J. Ebbert, G. Eichele, L.K. Estin, C. Faber, B.A. Facer, R. Fields, S.R. Fischer, T.P. Fliss, C. Frensley, S.N. Gates, K.J. Glattfelder, K.R. Halverson, M.R. Hart, J.G. Hohmann, M.P. Howell, D.P. Jeung, R.A. Johnson, P.T. Karr, R. Kawal, J.M. Kidney, R.H. Knapik, C.L. Kuan, J.H. Lake, A.R. Laramée, K.D. Larsen, C. Lau, T.A. Lemon, A.J. Liang, Y. Liu, L.T. Luong, J. Michaels, J.J. Morgan, R.J. Morgan, M.T. Mortrud, N.F. Mosqueda, L.L. Ng, R. Ng, G.J. Orta, C.C. Overly, T.H. Pak, S.E. Parry, S.D. Pathak, O.C. Pearson, R.B. Puchalski, Z.L. Riley, H.R. Rockett, S.A. Rowland, J.J. Royall, M.J. Ruiz, N.R. Sarno, K. Schaffnit, N.V. Shapovalova, T. Sivisay, C.R. Slaughterbeck, S.C. Smith, K.A. Smith, B.I. Smith, A.J. Sodt, N.N. Stewart, K-R. Stumpf, S.M. Sunkin, M. Sutram, A. Tam, C.D. Teemer, C. Thaller, C.L. Thompson, L.R. Varnam, A. Visel, R.M. Whitlock, P.E. Wohnoutka, C.K. Wolkey, V.Y. Wong, M. Wood, M.B. Yaylaoglu, R.C. Young, B.L. Youngstrom, X.F. Yuan, B. Zhang, T.A. Zwingman, and A.R. Jones. 2007. Genome-wide atlas of gene expression in the adult mouse brain. *Nature* 445: 168–76.

Lelièvre, S. A. 2009. Contributions of extracellular matrix signaling and tissue architecture to nuclear mechanisms and spatial organization of gene expression control. *Biochimica et Biophysica Acta* 1790(9): 925–35.

Lichtman, J., J. Livet, and J.R. Sanes. 2008. A technicolour approach to the connectome. *Nature Reviews Neuroscience* 9(6): 417–22.

Liewald, D., R. Miller, N. Logothetis, H.J. Wagner, and A. Schüz. 2014. Distribution of axon diameters in cortical white matter: An electron-microscopic study on three human brains and a macaque. *Biological Cybernetics* 108(5): 541–57.

Liu, X. 2012. Optogenetic stimulation of a hippocampal engram activates fear memory recall. *Nature* 484: 381–85.

Livet J., T.A. Weissman¹, H. Kang, R.W. Draft, J. Lu, R.A. Bennis, J.R. Sanes, and J.W. Lichtman. 2007. Transgenic strategies for combinatorial expression of fluorescent proteins in the nervous system. *Nature* 450: 56–62.

Lu, J.J.C. Tapia, O.L. White, and J.W. Lichtman. 2009. The interscutularis muscle connectome. *PLoS Biology* 7(4): e1000108.

MacAskill, A.F., J.E. Rinholm, A.E. Twelvetrees, I.L. Arancibia-Carcamo, J. Muir, A. Fransson, P. Aspenstrom, D. Attwell, and J.T. Kittler. 2009. Miro1 is a calcium sensor for glutamate receptor-dependent localization of mitochondria at synapses. *Neuron* 61: 541–55.

Mallouk, T. E., and A. Sen. 2009. Powering nanorobots. *Scientific American* 300: 72–77.

Ramaswami, S. J-D. Courcol, M. Abdellah, S.R. Adaszewski, N. Antille, S. Arsever, G. Atenekeng, A. Bilgili, Y. Brukau, A. Chalimourda, G. Chindemi, F. Delalandre, R. Dumusc, S. Eilemann, M.E. Gevaert, P. Gleeson, J.W. Graham, J.B. Hernando, L. Kanari, Y. Katkov, D. Keller, J.G. King, R. Ranjan, M.W. Reimann, C. Rössert, Y. Shi, J. C. Shillcock, M. Telefont, W.V. Geit, J.V. Diaz, R. Walker, Y. Wang, S.M. Zaninetta, J. DeFelipe, S.L. Hill, J. Muller, I. Segev, F. Schürmann, E.B. Muller, and H. Markram. 2015. The neocortical microcircuit collaboration portal: A resource for rat somatosensory cortex. *Frontiers in Neural Circuits* Vol 9, Article 44.

Markram, H. 2006. The Blue Brain Project. *Nature Reviews Neuroscience* 7: 153–160.

Martel, S., M. Mohammadi, O. Felfoul, Z. Lu, and P. Pouponneau. 2009. Flagellated magnetotactic bacteria as controlled MRI-trackable propulsion and steering systems for medical nanorobots operating in the human microvasculature. *International Journal of Robotics Research* 28(4): 571–82.

Martins, N.R.B., W. Erlhagen, and R.A. Freitas, Jr. 2012. Non-destructive whole-brain monitoring using nanorobots: Neural electrical data rate requirements. *International Journal of Machine Consciousness* 4: 109–140.

- Martins, N.R.B., W. Erlhagen, and R.A. Freitas, Jr. 2015. Action potential monitoring using neuronanorobots: Neuroelectric nanosensors. *International Journal of Nanomaterials and Nanostructures* 1: 20–41.
- Mavroides, D., and A. Ferreira, eds. 2011. *NanoRobotics: Current approaches and techniques*. New York: Springer.
- McAllister, A.K. 2007. Dynamic aspects of CNS synapse formation. *Annual Review of Neuroscience* 30: 425–50.
- Miyamoto, K. 1986. Numerical density estimation of mitochondria in thick slice by transmission emission microscopy. *Science on form: Proceedings of the First International Symposium for Science on Form*, 517–25. Tokyo: KTK Scientific Publishers.
- Modha-blog 2009. A proposal for mouse connectivity project.
http://p9.hostingprod.com/@modha.org/blog/2009/01/a_proposal_for_mouse_connectiv.html
 (accessed December 23, 2015).
- Mori, S., and J. Zhang. 2006. Principles of diffusion tensor imaging and its applications to basic neuroscience research. *Neuron* 51: 527–39.
- Morris, K. 2001. Macrodoctor, come meet the nanodoctors. *Lancet*. 357(9258): 778.
- Morris, R.L., and P.J. Hollenbeck. 1995. Axonal transport of mitochondria along microtubules and F-actin in living vertebrate neurons. *Journal of Cell Biology* 131: 1315–1326.
- Newman, E.A. 2001. Propagation of intercellular calcium waves in retinal astrocytes and Müller cells. *Journal of Neuroscience* 21(7): 2215–2223.
- NIH News. 2009. NIH Launches the Human Connectome Project to unravel the brain’s connections. Press release, July 16.
- Nopoulos, P., M. Flaum, D. O’Leary, and N.C. Andreasen. 2000. Sexual dimorphism in the human brain: Evaluation of tissue volume, tissue composition and surface anatomy using magnetic resonance imaging. *Psychiatry Research: Neuroimaging* 98(1): 1–13.
- Okabe S. 2007. Molecular anatomy of the postsynaptic density. *Molecular and Cellular Neuroscience* 34(4): 503–518.
- Pakkenberg, B., and H.J.G. Gundersen. 1997. Neocortical neuron number in humans: Effect of sex and age. *Journal of Comparative Neurology* 384: 312–320.
- Palmer, L. M., and G. J. Stuart. 2006. Site of action potential initiation in Layer 5 pyramidal neurons. *Journal of Neuroscience* 26(6): 1854–1863.
- Park, H.H., A.C. Jamison, and T.R. Lee. 2007. Rise of the nanomachine: The evolution of a revolution in medicine. *Nanomedicine* 2(4): 425–39.
- Patel, G.M., G.C. Patel, R.B. Patel, J.K. Patel, and M. Patel. 2006. Nanorobot: A versatile tool in nanomedicine. *Journal of Drug Targeting* 14(2): 63–67.
- Perrot, R., R. Berges, A. Bocquet, and J. Eyer. 2008. Review of the multiple aspects of neurofilament functions, and their possible contribution to neurodegeneration. *Molecular Neurobiology* 38(1): 27–65.
- Popov, A.M., Y. E Lozovik, S. Fiorito, and L’H. Yahia. 2007. Biocompatibility and applications of carbon nanotubes in medical nanorobots. *International Journal of Nanomedicine* 2(3): 361–72.

- Qu, L., Y. Akbergenova, Y. Hu, and T. Schikorski. 2009. Synapse-to-synapse variation in mean synaptic vesicle size and its relationship with synaptic morphology and function. *Journal of Comparative Neurology* 514(4): 343–52.
- Rácz, B., T.A. Blanpied, M.D. Ehlers, and R.J. Weinberg. 2004. Lateral organization of endocytic machinery in dendritic spines. *Nature Neuroscience* 7: 917–18.
- Rengachary, S.S., and R.G., Ellenbogen, eds. 2005. *Principles of neurosurgery*. Amsterdam: Mosby-Elsevier.
- Rollenhagen, A., and J.H.R. Lübke. 2006. The morphology of excitatory central synapses: From structure to function. *Cell Tissue Res* 326: 221–37.
- Rollenhagen, A., K. Sätzler, E.P. Rodríguez, P. Jonas, M. Frotscher, and J.H. Lübke. 2007. Structural determinants of transmission at large hippocampal mossy fiber synapses. *Journal of Neuroscience* 27(39): 10434–10444.
- Sabatini, B.L., and W.G. Regehr. 1996. Timing of neurotransmission at fast synapses in the mammalian brain. *Nature* 384: 170–72.
- Sala, C., I. Cambianica, and F. Rossi. 2008. Molecular mechanisms of dendritic spine development and maintenance. *Acta Neurobiologiae Experimentalis* 68(2): 289–304.
- Sandberg, A., and N. Bostrom. 2008. Whole brain emulation: A roadmap. Technical report. Future of Humanity Institute, Oxford University.
- Scheff, S.W., and D.A. Price. 2006. Alzheimer's disease-related alterations in synaptic density: Neocortex and hippocampus. *Journal of Alzheimer's Disease* 9(3 Suppl): 101–115.
- Schwarz, T.L. 2013. Mitochondrial trafficking in neurons. *Cold Spring Harbor Perspectives in Biology* 5(6): 5:a011304.
- Seung, H.S. 2010. TED Talks – Sebastian Seung: I am my connectome. July, 2010. Oxford, England.
- Seung, H.S. 2011. Neuroscience: Towards functional connectomics. *Nature* 471: 170–72.
- Sheng, M., and C.C. Hoogenraad. 2007. The postsynaptic architecture of excitatory synapses: A more quantitative view. *Annual Review of Biochemistry* 76: 823–47.
- Sheng, Z. H. 2014. Mitochondrial trafficking and anchoring in neurons: New insight and implications. *Journal of Cell Biology* 204(7): 1087–1098.
- Shepherd, G.M.G., and K.M. Harris. 2010. Three-dimensional structure and composition of CA3/CA1 axons in rat hippocampal slices: Implications for presynaptic connectivity and compartmentalization. *Journal of Neuroscience* 18(20): 8300–8310.
- Shin, S.S., T. Verstynen, S. Pathak, K. Jarbo, A.J. Hricik, M. Maserati, S.R. Beers, A.M. Puccio, F.E. Boada, D.O. Okonkwo, and W. Schneider. 2012. High-definition fiber tracking for assessment of neurological deficit in a case of traumatic brain injury: Finding, visualizing, and interpreting small sites of damage: Case report video. *Journal of Neurosurgery* 116(5): 1062–1069.
- Smith, S.M., R. Renden, and H. von Gersdorff. 2008. Synaptic vesicle endocytosis: Fast and slow modes of membrane retrieval. *Trends in Neurosciences* 31(11): 559–68.
- Spacek, J. 2006. Comparative morphology of dendritic spines and spine synapses. From: Synapse Web.
- Spacek, J., and K. Sorra. 2007. Synapses of stratum radiatum. Synapse. <http://synapses.clm.utexas.edu/anatomy/radiatum/synapses.stm> (accessed December 23, 2015).

- Sporns, O., G. Tononi, and R. Kötter. 2005. The human connectome: A structural description of the human brain. *PLoS Computational Biology* 1(4): e42.
- Südhof, T.C. 2004. The synaptic vesicle cycle. *Annual Review of Neuroscience* 27: 509–547.
- Sun, T., H. Qiao, P-Y. Pan, Y. Chen, and Z-H. Sheng. 2013. Motile axonal mitochondria contribute to the variability of presynaptic strength. *Cell Reports* 4: 413–419.
- Syková, E., and C. Nicholson. 2008. Diffusion in brain extracellular space. *Physiology Reviews* 88: 1277–1340.
- Terry, R.D., E. Masliah, D.P. Salmon, N. Butters, R. DeTeresa, R. Hill, L.A. Hansen, and R. Katzman. 1991. Physical basis of cognitive alterations in Alzheimer's disease: Synapse loss is the major correlate of cognitive impairment. *Annals of Neurology* 30(4): 572–80.
- Theodore, T.W., R. Preissl, P. Datta, M. Flickner, R. Singh, S.K. Esser, E. McQuinn, R. Appuswamy, W.P. Risk, H.D. Simon, and D.S. Modha. 2012. 10¹⁴, IBM Research Report. Weblink: [http://domino.research.ibm.com/library/cyberdig.nsf/papers/19B9020D53E753DB85257AB7005FFA18/\\$File/RJ10502.pdf](http://domino.research.ibm.com/library/cyberdig.nsf/papers/19B9020D53E753DB85257AB7005FFA18/$File/RJ10502.pdf) (accessed December 23, 2015)
- Thorne, R.G., and C. Nicholson. 2006. *In vivo* diffusion analysis with quantum dots and dextrans predicts the width of brain extracellular space. *Proceedings of the National Academy of Sciences* 103: 5567–5572.
- Tkachuk, A., F. Duewer, H. Cui, M. Feser, S. Wang, and W. Yun. 2007. X-ray computed tomography in Zernike phase contrast mode at 8 keV with 50-nm resolution using Cu rotation anode X-ray source. *Zeitschrift für Kristallographie* 222(11): 650–55.
- Trachtenberg, J.T. 2002. Long-term *in vivo* imaging of experience-dependent synaptic plasticity in adult cortex. *Nature* 420: 788–94.
- Travis E. R., and R. M. Wightman. 1998. Spatio-temporal resolution of exocytosis from individual cells. *Annual Review of Biophysics and Biomolecular Structure* 27: 77–103.
- Trushina, E., E. Nemetlu, S. Zhang, T. Christensen, J. Camp, J. Mesa, A. Siddiqui, Y. Tamura, H. Sesaki, T.M. Wengenack, P.P. Dzeja, and J.F. Poduslo. 2012. Defects in mitochondrial dynamics and metabolomic signatures of evolving energetic stress in mouse models of familial Alzheimer's disease. *PLoS ONE* 7(2): e32737.
- Vaidyanathana, M., L.P. Clarke, C. Heidtman, R.P. Velthuisen, and L.O. Hall. 1997. Normal brain volume measurements using multispectral MRI segmentation. *Magnetic Resonance Imaging* 15(1): 87–97.
- Varshney, C., B.L. Chen, E. Paniagua, D.H. Hall, and D.B. Chklovskii. 2011. Structural properties of the *C. elegans* neuronal network. *PLoS Computational Biology* 3(7): e1001066.
- White, J.G., E. Southgate, J.N. Thomson, and S. Brenner. 1986. The structure of the nervous system of the nematode *Caenorhabditis elegans*. *Philosophical Transactions of the Royal Society B: Biological Sciences* 314: 1–340.
- Wormatlas. 2008. Wormatlas: A database featuring behavioral and structural anatomy of *Caenorhabditis elegans*. <http://wormatlas.org/> (accessed December 23, 2015).
- Zador, A., J. Dubnau, H.K. Oyibo, H. Zhan, G. Cao, and I.D. Peikon. 2012. Sequencing the connectome. *PLoS Biology* 10(10): e1001411.
- Zuo, Y., A. Lin, P. Chang, and W-B. Gan. 2005. Development of long-term dendritic spine stability in diverse regions of cerebral cortex. *Neuron* 46(2): 181–89.